Clastic dikes in the Dead Sea basin as indicators of local site amplification

Y. Jacoby, R. Weinberger, T. Levi & S. Marco

Natural Hazards
Journal of the International Society for the Prevention and Mitigation of Natural Hazards

ISSN 0921-030X
Volume 75
Number 2

Nat Hazards (2015) 75:1649-1676
DOI 10.1007/s11069-014-1392-0

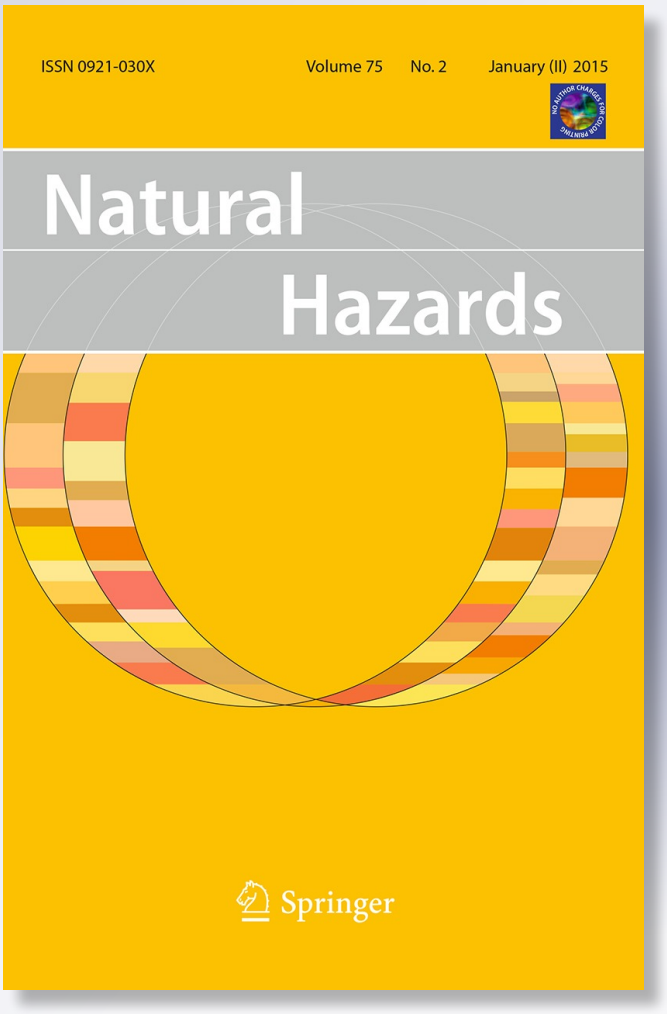

Springer

Nat Hazards (2015) 75:1649–1676
DOI 10.1007/s11069-014-1392-0

ORIGINAL PAPER

Clastic dikes in the Dead Sea basin as indicators of local site amplification

Y. Jacoby · R. Weinberger · T. Levi · S. Marco

Received: 28 October 2013 / Accepted: 11 August 2014 / Published online: 7 September 2014

Abstract Early Holocene seismic activity triggered fluidization and clastic-dike emplacement within Late Pleistocene lacustrine Lisan Formation sediments in the Dead Sea basin (DSB). Hundreds of opening-mode clastic dikes were documented cross-cutting the Lisan Formation in four distinct sites in relatively small (<5 km^2) areas: Bet ha'Arava, Masada Plain, Ami'az Plain, and Nahal Amazyahu. The spatial distribution of clastic-dike sites, although limited to Lisan Formation outcrops, still indicates wide-scale distribution. All sites were demonstrated similarly in site dimensions, geometric parameters, dike infill materials, anisotropy of magnetic susceptibility (AMS) fabrics, and spatial distribution patterns of clastic dikes. Field observations and laboratory analyses (grain size, XRD, and AMS) indicate transport of clastics from source layers below, indicating that dike emplacement was associated with the fluidization of lower Lisan clay-rich sediments. In all of the sites, the clastic dikes show a wide range of directions with clustered orientations, which might have been dictated by the local stress field that prevailed during dynamic fracturing of the Lisan host rock. Peak ground velocities were calculated for the Ami'az Plain by using a range of earthquake magnitudes and epicentral distances. The analyses indicate that liquefaction of features such as clastic dikes is related to amplification of seismic waves in specific sites, and the sites locations are up to 60 km away from an epicenter in moderate earthquakes ($M_w \leq 6.5$), and more than 60 km away from an epicenter in strong earthquakes ($M_w > 6.5$). The injection of clastic dikes in distinct and relatively small areas in the Lisan Formation along the DSB may serve as evidence for a unique combination of three factors: (a) clay-rich sediments and high water table as

Y. Jacoby (✉) · S. Marco
Department of Geophysics and Planetary Sciences, Tel-Aviv University, 69978 Tel Aviv, Israel
e-mail: yael.j.g@gmail.com

R. Weinberger · T. Levi
Geological Survey of Israel, 30 Malkhe Israel, 95501 Jerusalem, Israel

R. Weinberger
Department of Geological and Environmental Sciences, Ben Gurion University of the Negev, 84105 Beer Sheba, Israel

favorable conditions for fluidization on the exposed surface following the Lake Lisan regression; (b) the occurrence of moderate-to-strong earthquakes ($M_w > 6$) in the early Holocene after the deposition of the Lisan Formation; and (c) the local geological structure characterized by edge and basin effects, which can amplify seismic waves. The present study indicates that injection due to fluidization of clay-rich strata during earthquakes was dominant throughout the DSB. We suggest that the clastic dikes can serve as evidence for local amplification conditions following seismic processes that occur close to active faults.

Keywords Clastic dikes · Dead Sea Transform · Seismites · Amplification · Anisotropy of magnetic susceptibility

1 Introduction

Hazards next to the Dead Sea Transform (DST), like near other plate boundary systems, may vary due to local amplification of seismic waves in defined structural areas. One expression of the hazards may be sought in the response of the uppermost strata in the form of brittle deformation. To this end, we examined the spatial distribution of clastic dikes that crosscut the Lisan Formation (Begin et al. 1980) in the Dead Sea basin (DSB) along the central sector of the DST.

Clastic dikes are opening-mode fractures, indicating brittle fracturing of the host rock (e.g., Pollard and Aydin 1988; Vermilye and Scholz 1995); they are discordant, sub-vertical sheets of sediment within a contrasting host rock. The transport of clastic material into clastic dikes is considered evidence for their dynamic formation process. While the final geometry of these clastic dikes shows similarities everywhere and is usually well defined, their mode of formation is commonly ambiguous. This ambiguity arises because the sediment comprising the clastic dikes may accumulate either "passively" by deposition of clastic materials into preexisting fissures (Eyal 1988) or "dynamically" by fracturing the country rocks and injection of clastic materials during overpressure buildup (Jolly and Lonergan 2002). Injection dikes commonly form during earthquakes that trigger fracturing, fluidization, and injection of clastics into fractures (e.g., Obermeier 1998; Galli 2000; Levi et al. 2006a, b, 2008, 2009). A passive deposition of clastic material into preexisting fissures is also common (Borradaile 1984; Eyal 1988) and relatively easy to discern (lack of connection with source layer, texture not evidencing upward flow, absence of fragments of host material, etc.). The orientations of clastic dikes are coaxial either with a regional stress field (Huang 1988; Loveless et al. 2005, 2009) or a local stress field (Marco et al. 2002) or superposition of both (Gardosh 1987; Neal et al. 1968). Hence, clastic dikes are considered as a useful tool for reconstructing the stress field at the time of emplacement. Clastic dikes may form during strong, earthquake-induced, ground motion (McCalpin 1996), close (<50 km) to the epicenter (Galli 2000), and may be enhanced by special structural conditions (Celebi 1991). Olson et al. (2005 and references therein) presented a magnitude-bound curves for varying geographic and tectonic settings. They indicated that earthquake-induced liquefaction features as sandy clastic dikes can be used for locating palaeo-epicenters. Using empirical relationships, Reicherter et al. (2009) and Serva et al. (2011) evaluated the minimum ground motion of an earthquake that induced injected clastic dikes within 50 km of the epicenter. Further away from the epicenter, clastic dikes may also be emplaced, if special structural conditions lead to ground motion amplifications.

Previous studies in the Ami'az Plain (Marco et al. 2002; Levi et al. 2006a, b, 2008) demonstrated that fluidized clay-rich clastics of the Late Pleistocene lacustrine Lisan Formation were injected from source layers into fractures during strong ($M_w > 6.5$) earthquakes in early Holocene times. These earthquake-induced clastic dikes are located within the seismically active DSB (Fig. 1a). Based on fracture- and fluid mechanics models, Levi et al. (2008) calculated that during the injection process, the overpressure within the source layers was between 1 and 10 MPa and the dike propagation velocity reached tens of meters per second. These figures are relatively high compared to the lithostatic pressure of the surrounding host rock (<0.5 MPa) and the propagation velocity of magmatic dikes (up to several meters per second).

Fluidization of clay-rich sediment could occur (e.g., Levi et al. 2006a), but this mechanism is not well studied and might differ from fluidization and liquefaction process of sandy sediments (e.g., Yilmaz et al. 2004, and references therein). For instance, Heifetz et al. (2005) suggested that liquefaction in soft sediment might occur immediately after the main shock by shear stresses acting on the interface between two layers that induce Kelvin–Helmholtz instability. Bachrach et al. (2001) suggested that liquefaction in soft sediment can be a direct result of the shock waves, compatible with loading by *P* waves, without the need of an indirect shear displacement mechanism and induced porosity reduction.

The natural in situ water (brine) content of the green clayey Lisan source sediment is between 27 and 36 %, which is within or close to the range obtained from the maximum liquid content of this sediment (Arkin and Michaeli 1986). Injection of the infill material transported from the Lisan source sediment layer several meters below the surface is caused by a fluidization process (without a reduction pore process), which is associated with a pressure buildup process and its relation to the dynamic stresses generated during earthquakes (Levi et al. 2008).

Based on the resetting of optically stimulated luminescence (OSL) signals of quartz grains, Porat et al. (2007) suggested that the clastic dikes in the Ami'az Plain were emplaced between 15 and 7 ky B.P. Begin et al. (2005) compared the paleoseismic record with the present seismicity in the Dead Sea area; their extrapolation to $M > 6.5$ shows a recurrence interval of 1,000 year. Hamiel et al. (2009) calculated from a combined record an average recurrence interval of 500 year for strong earthquakes ($M_w \geq 6.5$) in the DSB.

In the present study, we focus on the spatial distribution of the clastic dikes in the DSB and discuss their importance in identifying areas which are prone to high ground amplification during earthquakes. We first studied the origin of the clastic dikes by applying several techniques, including field observations, measurement of anisotropy magnetic susceptibility (AMS), and study of the grain-size and mineralogical assemblage of the dike infill. In order to characterize the clastic dikes and assess the stress field that prevailed during their emplacement, we mapped and measured the clastic dikes and their orientations in four areas along the DSB. We then synthesized the available structural data and explored the distinct clustering of clastic dikes in the DSB.

2 Geological setting

2.1 General

The DST is an active strike-slip fault connecting the East Anatolian fault in the north with the extensional zone of the Red Sea rifting in the south (Fig. 1a; Garfunkel et al. 1981). It

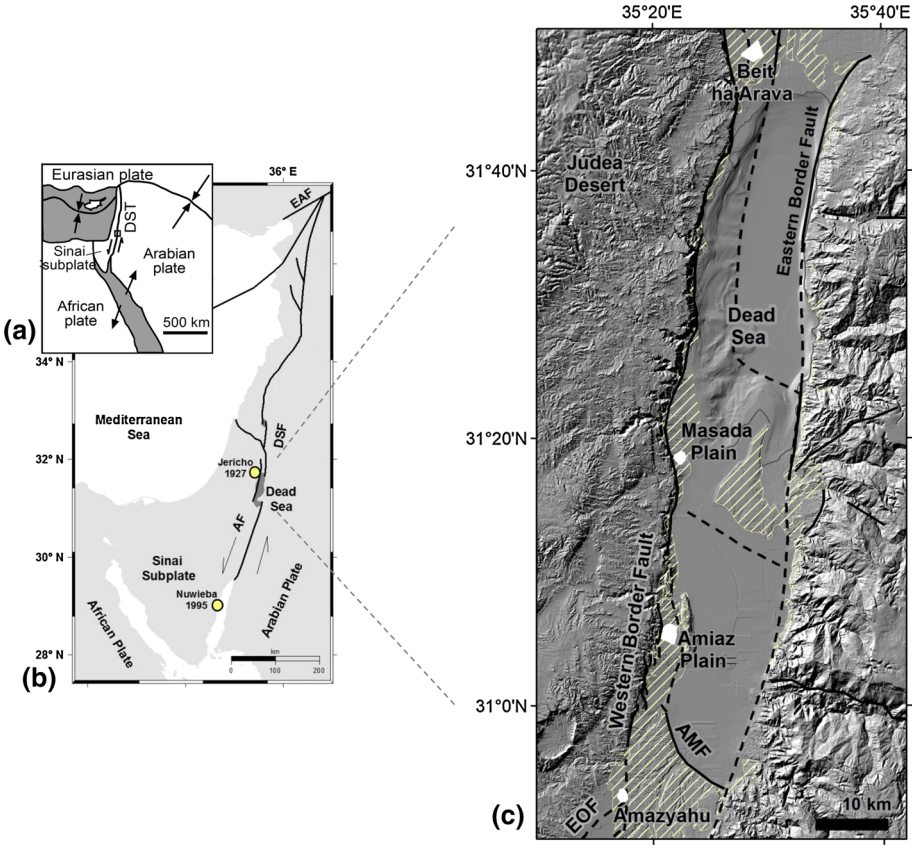

Fig. 1 **a** Configuration of tectonic plates in the Middle East. *DST* Dead Sea Transform, *EAF* East Anatolian Fault. **b** *Map* showing the geological setting of the study areas next to the DST modified after Garfunkel et al. (1981). Epicenters of the 1927 Jericho (Shapira et al. 1993; Avni et al. 2002) and 1995 Gulf of Aqaba (Hofstetter 2003) earthquakes are marked with *yellow circles*. **c** Locations of the study areas (*white-colored polygons*) and Lisan Formation outcrops dispersion (diagonal lines overlay) on the backdrop of a *shaded relief map* of the DSB (Hall 1993). The Eastern and the Western border faults and the Amazyahu faults are marked by *heavy dashed line*; the shore of the present Dead Sea is marked by a *thin solid line*. Faults modified after Sneh and Weinberger (2014). *EAF* East Anatolian Fault, *DST* Dead Sea Transform, *AF* Arava Fault, *AMF* Amazyahu Fault, *EOF* En Ofarim Fault

defines the active boundary between the Arabian and the African (Sinai) plates with an estimated slip rate of ~3–5 mm/year (Wdowinski et al. 2004; Marco et al. 2005; Le Beon et al. 2008). The ~105 km left-lateral motion along the DST since its formation in the Early–Mid Miocene (Quennell 1958; Freund et al. 1968) created several pull-apart basins, the largest of which is the DSB (Fig. 1a).

The DSB is bounded by a series of oblique-normal step-faults. It is filled with ~10 km of lacustrine and fluvial sediments, in places penetrated by large salt diapirs (Weinberger et al. 2006). It is generally accepted that both the Eastern and Western Border faults (WBF) (Fig. 1b) bounding the basin are active (Aldersons et al. 2003; Hofstetter et al. 2007; Data and Resources).

Clastic dikes were previously described at the western margins of the DSB by Gardosh (1987), Neev and Emery (1995), Marco et al. (2002), Davis (2007), and Levi et al. (2006a, b, 2008, 2009, 2011). Almost all the observed clastic dikes are emplaced within the Lisan Formation.

The Lisan Formation is composed of ~40-m-thick lacustrine deposits, consisting mostly of authigenic aragonite laminae, alternating with fine detritus layers (Begin et al. 1980). The clay-rich layers of the Lisan Formation are up to 0.5 m thick. The upper part of the formation consists of a ~1-m-thick, relatively stiff, gypsum layer. The U–Th age of the Lisan Formation ranges from ~70,000 to 15,000 years B.P. (Haase-Schramm et al. 2004). The Lisan Formation overlies the Samra Formation (Picard 1943), which was deposited between ~140 and 75 ka (Waldmann et al. 2007).

2.2 Seismicity along the Dead Sea Transform

Moderate and strong earthquakes associated with the DST appear in geological, historical, and archaeological records. The DST system has been the source of intensive earthquake activity affecting Israeli territory (Fig. 1b), including the destructive earthquake $M_w = 6.2$ in 1927 (Shapira et al. 1993; Avni et al. 2002) and the major $M_w = 7.1$ earthquake in 1995 (e.g., Hofstetter 2003).

Paleoseismic records are preserved in lacustrine sediments in the Dead Sea region. They exhibit several deformation structures: (1) syn-sedimentary faults (Marco and Agnon 1995, 2005); (2) folds and faults generated during soft-sediment slumping and deformation (Alsop and Marco 2011, 2012 and references therein); (3) breccia beds in the Lisan Formation and in the Holocene Ze'elim Formation induced by $M > 5.5$ earthquakes (Marco and Agnon 1995; Marco et al. 1996; Marco and Agnon 2005; Ken-Tor et al. 2001); (4) clastic dikes (Marco et al. 2002; Levi et al. 2006a). The emplacement of earthquake-induced clastic dikes in the Ami'az Plain must have been related to relatively high ground motion, which triggered injection of clastic material (Levi et al. 2006a, b); and (5) appearance of large asphalt blocks that seep out through faults and fissures at the bottom of the lake after strong earthquakes (Ben-Menahem 1991).

2.3 Structural setting of the study areas (Table 1)

The *Bet ha'Arava* area is located at the northwestern part of the Dead Sea area. It is situated on a downfaulted block between the Dead Sea WBF and the Jericho fault. The latter is the main strand of the DST in this area (Fig. 2a). The Bet ha'Arava block is characterized by a north–south elongated domal shape as seen on the local structural map of the top Judea Group, dated to the Turonian (Fig. 2a). High velocity reflective layers of rock salt (i.e., Sedom salt) overlie the Judea Group (Belitzky and Mimran 1996; Shamir 2006). Shamir et al. (2005) identified a salt layer at 900–1,500 m below sea level, with average P wave velocities of 1,500–2,500 m/s, respectively.

The *Masada Plain* is situated over a downfaulted block between the Dead Sea WBF and an intrabasinal normal fault within the Dead Sea. A structural map of the top Sedom salt is presented in Fig. 2b, showing gentle tilting eastward (Israel National Oil Company 1999). The syn-Lisan Masada fault zone (Marco et al. 1996) comprises ~N–S-trending faults parallel to the WBF. This fault zone was traced by high-resolution seismic reflections down to 250 m (Marco et al. 1996; Agnon et al. 2006), which is evidence for syn-depositional faulting.

Table 1 Table presenting geometric and structural setting data of the study areas

	Bet ha'Arava	Masada Plain	Ami'az Plain	Nahal Amazyahu
Area (km^2)	2.7	3.5	3.5	1.0
Number of dikes	149	130	250	230
Main clustering directions	NNE, NNW	NW, N	ENE, W, NNW	NE,W, NW
Possible reflector structure	Dome margin on downfaulted block	Downfaulted block	Center of sub-basin	Downfaulted block
Presence of other seismites	−	+	+	−
Elevation of top Lisan Fm. (m.s.l.)	−290	−330	−260	−290

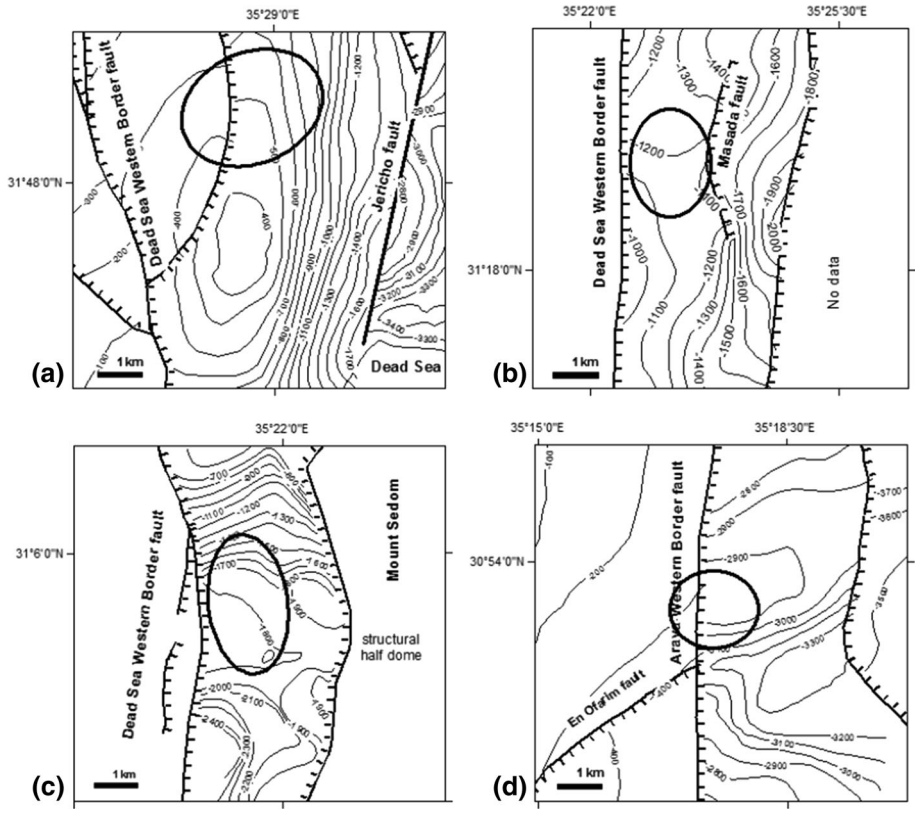

Fig. 2 **a** Structural map of the top Judea Group in the Bet ha'Arava area; contour interval is 100 m (Fleischer et al. 2001). The site is situated on a downfaulted block 3 km west of the Jericho fault, on a dome structure bordered by two normal faults within the Jericho basin. **b** Structural map of the top Sedom Formation (i.e., rock salt beds) in the Masada Plain; contour interval is 100 m (Israel National Oil Company 1999). The Masada Plain is situated between the Western Border fault and a 20-m erosional escarpment of the Lisan Formation in the downfaulted block. **c** Structural map of the top Sedom Formation in the Ami'az Plain; contour interval is 100 m (Israel National Oil Company 1992). The Amiaz Plain is situated on a downfaulted block next to the Western Border Fault. The Mount Sedom salt diapir forms a positive relief to the east. **d** Structural map of the top Judea Group in the northern Arava Valley; contour interval is 100 m (Fleischer and Gafsou 1998). The study area is situated on the Western Border Fault in the northern Arava Valley, about 2 km north of the intersection between the main fault and the En Ofarim Fault

The *Ami'az Plain* is situated over a downfaulted block in the western margin of the DSB and is bounded by the WBF on the west and the Mount Sedom salt diapir on the east. A structural map of the top Sedom salt 0.6–2.5 km below the surface, dated to Pliocene age (Zak 1967), shows a southward tilting, elongated syncline, forming a narrow ($\sim$3 km) sub-basin within the DSB (Fig. 2c, Israel National Oil Company 1992).

The *Nahal Amazyahu* area is situated over the downfaulted block next to the Arava WBF, 2 km north of the En Ofarim fault intersection (Fig. 2d). The structural map of the top Judea Group (Fig. 2d, Fleischer and Gafsou 1998) shows a downfaulted block with an anticline/syncline system. The site is overlying the anticline, which is located 2.8 km below the surface east of the Arava WBF.

3 Methods and sampling strategy

3.1 Field and aerial photograph mapping

The fieldwork included the measurement of clastic-dike directions, and their heights and widths. We documented the stratigraphic levels of the Lisan Formation in which the clastic dikes are recognized, as well as their possible physical connection to the source layers. Complementary measurements of clastic-dike strikes were made using aerial photographs. Directions are presented in rose diagrams and in statistic circular orientation dispersal (Appendix). In each study area, we quantified the observed areal size in which clastic dikes were emplaced. In order to test the possibility that the spatial distribution of clastic dikes is associated with deep-seated structures, the quantification process was done on the backdrop of existing structural maps. The measurement of the total area affected by dikes (Table 1) could be indicative of the surficial deformation size that formed during the earthquake events.

3.2 Measurements of low-field magnetic susceptibility

For characterizing the magnetic fabric of the clastic dikes, we sampled 66 specimens from ***10*** dikes: Bet ha'Arava—19 specimens from three dikes; Masada Plain—15 specimens from two dikes; and Nahal Amazyahu area—32 specimens from five dikes. The AMS fabrics of clastic dikes in the Ami'az Plain were previously studied by Levi et al. (2006a, b). The dikes were sampled across their width and along their height by carving $2 \times 2 \times 2$ cm cubic pedestals with a sharp knife.

The magnetic susceptibility indicates the capacity of the material to be magnetized in an applied magnetic field. In an anisotropic material, the magnetic susceptibility (k) relates the applied magnetic field (H) to an induced magnetization (M) by $M = kH$. In tensorial notation, this equation can be written as follows: $M_i = k_{ij}H_j$, where M_i is the magnetization vector, k_{ij} is the susceptibility matrix, and H_j is the applied field vector. The shape of the anisotropy of magnetic susceptibility (AMS) is described by the three principal values k_{max} (k_1), k_{int} (k_2), and k_{min} (k_3), which correspond to the maximum, intermediate, and minimum magnetic susceptibility magnitudes, respectively (Borradaile and Jackson 2004).

In the present study, the AMS method (e.g., Borradaile and Henry 1997) was applied in order to distinguish between depositional and injection clastic dikes and to determine the kinematics and the flow directions of the injected clastics (Tauxe 1998; Levi et al. 2006a). A depositional clastic dike is characterized by an oblate AMS ellipsoid and well-grouped vertical k_3 axes (known as "deposition fabric"). An injection clastic dike is characterized by a triaxial AMS ellipsoid and well-grouped sub-horizontal and/or sub-vertical AMS axes (known as "flow fabric"). Similar to AMS fabrics in magmatic dikes (Moreira et al. 1999; Féménias et al. 2004), the "flow fabric" in injection dikes can be characterized by particle imbrications along the dike's walls. For example, under high-energy flow conditions with vertical transport of clastic materials, the evolved fabric is associated with well-grouped sub-vertical k_2 axes and sub-horizontal k_1 and k_3 axes. For additional examples and categorizations of flow conditions and related AMS fabrics in clastic dikes see Levi et al. (2006b, text and Fig. 3).

3.3 Mineralogical composition and grain size

We studied the mineralogy and grain-size distribution of 15 representative samples from 13 clastic dikes and 2 source layers. These analyses helped to relate a particular dike infill to a potential source layer, as well as to compare between the mineralogical components and the grain-size distribution of the dike infill at different localities.

The mineralogy was determined by X-ray diffraction at the Geological Survey of Israel (GSI). The analyses were carried out on a Philips XRD PW1830/3710/3020 diffractometer. Semi-quantitative estimates of the mineralogy were determined by comparison with calibration curves and the corresponding chemical composition. Grain-size analyses were performed by the Mastersizer Laser (Malvern MS-2000) at the GSI. To avoid clay aggregation, dry sediment samples were mixed with 25 ml distilled water with Calgon.

3.4 Liquefaction potential simulation

A quantitative simulation for evaluating liquefaction potential depends on a hypothetical peak ground velocity (PGV) in the Ami'az Plain, and was performed with the HAZUS software (FEMA and NIBS 2012). The simulation involves a prediction of peak ground velocity generated by hypothetical earthquakes of various magnitudes (6–7.5 M_w) and ranges of epicentral distances (3, 10, 20, 40, 60, and 90 km), which might generate the distribution of the liquefaction features. Ground velocity threshold values for liquefaction and fluidization structures are based on documented velocities (Cowan 1999; Kostadinov and Towhata 2002; Guo et al. 2006).

The estimations of the peak ground velocity (PGV) in the Ami'az Plain are based on the attenuation equation of Campbell and Bozorgnia (2008), which is currently applied in Israel (Klar et al. 2011). The PGVs are calculated for a synthetic faults and different epicentral distances (3, 10, 20, 40, 60, and 90 km from the epicenter location), by two scenarios—with and without amplification. The present estimations of PGV are based on the amplification factor published by Shani-Kadmiel et al. (2012, 2014). They show that the amplification is triggered by "basin effect" (Shani-Kadmiel et al. 2012) and "focusing effect" (Shani-Kadmiel et al. 2014) very close to the surface. They calculate an amplification factor in about 3 (see Fig. 2g in Shani-Kadmiel et al. 2012; and in Fig. 4j in Shani-Kadmiel et al. 2014), which is used in the present study. A minimum PGV threshold for liquefaction represents the critical value for triggering liquefaction of clay-rich soils. For liquefaction features such as clastic dikes, we use PGV = 0.1 m/s, which is estimated to be the minimum PGV to induce liquefaction (Cowan 1999; Kostadinov and Towhata 2002) and fluidization (0.04–0.13 m/s; Guo et al. 2006).

4 Results

4.1 Field observations

The clastic dikes are observed almost only in the Lisan Formation. They are usually exposed along canyon walls and gypsum benches within the Lisan host rock. Geomorphic features such as sinkholes, gullies, and incisions are usually associated with the clastic dikes and are governed by the directions of the clastic dikes. Summaries of the field measurements are presented in Tables 1 and 2.

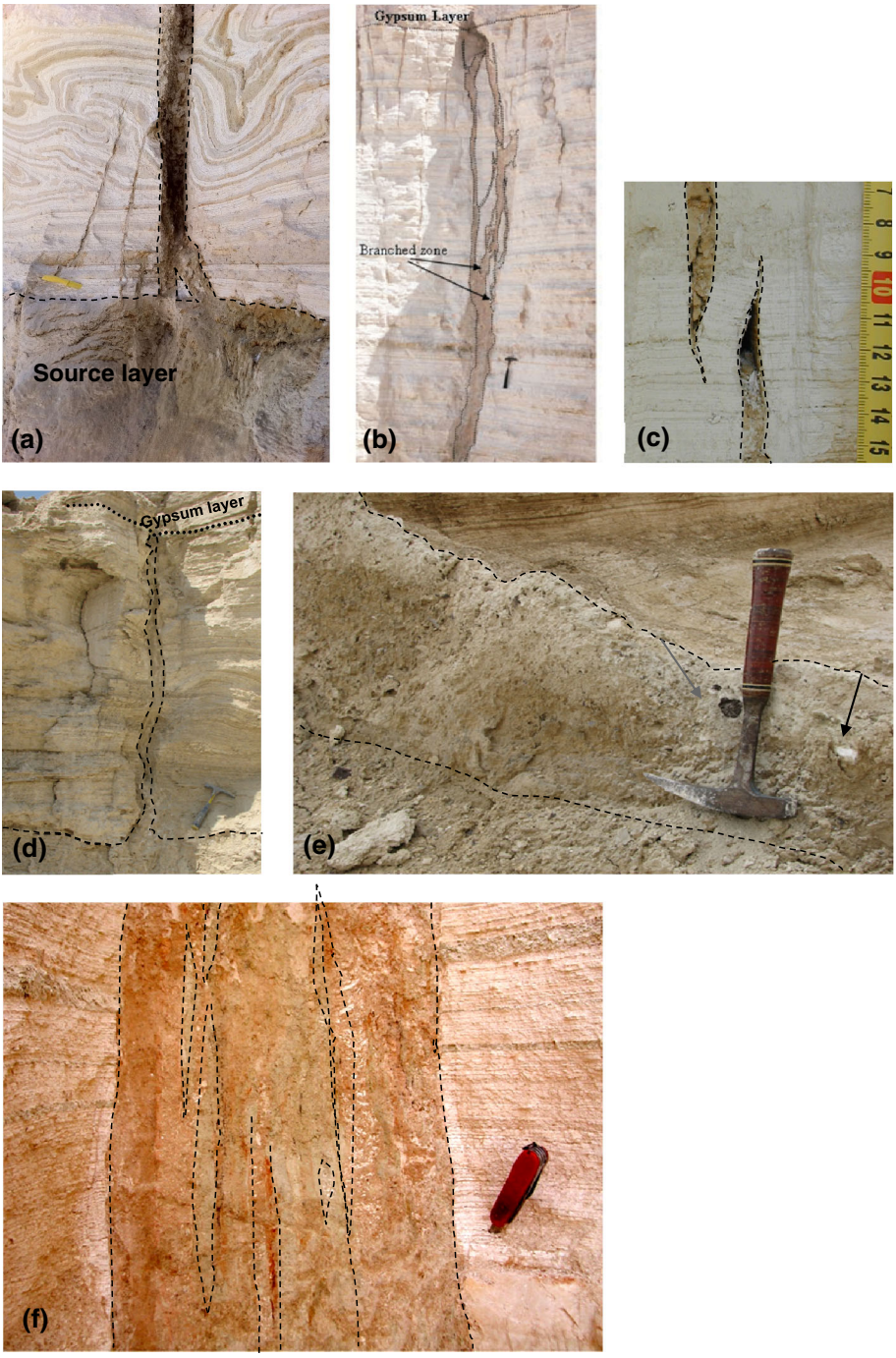

The majority of the dikes terminate against a 0.5-m-thick gypsum layer at the top of the Lisan section, but some continue up to the surface. They are commonly filled with green clay, silty quartz, and fragments of Lisan Formation laminae. Many of the injection dikes

◀**Fig. 3** **a** Physical connection between a clastic dike and the Lisan source layer 6 m below the surface in the Ami'az Plain. Source layer thickness is ~0.4 m. *Yellow knife* indicates scale. **b** Clastic dike in the Ami'az Plain filled with clastic material, crosscutting the Lisan Formation about 12–18 m above its source layer. The dike branches upward into several strands (locations marked by *arrows*), which occasionally coalesce upward. Geological hammer indicates scale. **c** Two overlapping dikelets at the *upper part* of the Lisan Formation, Masada Plain, indicating local sub-horizontal transport of clastics. **d** Clastic dike in Bet ha'Arava, filled with *green clay* sediments, crosscuts the upper Lisan Formation and terminates against a stiff gypsum layer. Geological hammer indicates scale. **e** Clastic dike in the Masada Plain contains pebbles derived from Lisan layers rich in detritus (see *black arrow*) and decorated with discrete pieces of asphalt and oil films (see *gray arrow*). Geological hammer indicates scale. **f** Clastic dike in the Amiaz Plain composed of a few vertical layers. Pocket knife indicates scale

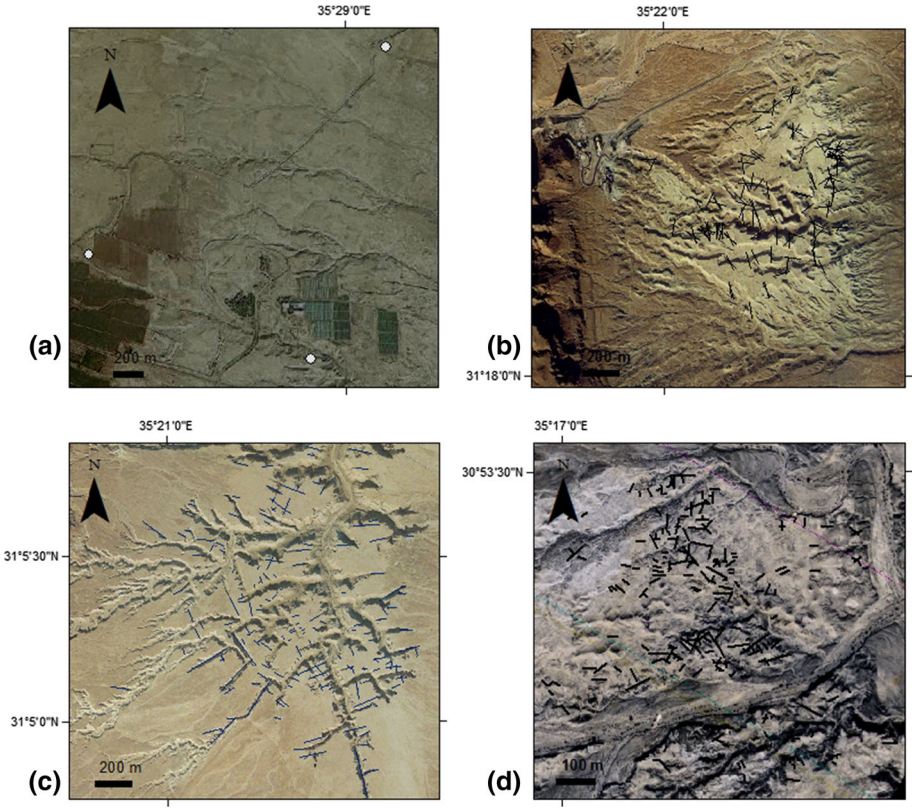

Fig. 4 **a** Aerial photograph of Bet ha'Arava area showing the study sites of exposed clastic dikes. The area was intensively cultivated over the last decades, which inhibited marking the clastic dikes observed previously by Gardosh (1987). Aerial photograph with marked trace of exposed clastic dikes in **b** Masada Plain, **c** Ami'az Plain, and **d** Nahal Amazyahu

are composed of several segments, some of which branch toward the surface and split into 3–5 large strands (Fig. 3b). In the Ami'az Plain, Masada Plain, and Bet ha'Arava, many of the larger clastic dikes (>10 m, height) are accompanied by numerous, much smaller dikelets (<1 m, height) (Fig. 3c). The dike infill commonly consists of vertical layers (Fig. 3f).

Table 2 Table presenting the dike geometric parameters in all sites, their infill materials, mineralogy, and AMS fabric

	Bet ha'Arava	Masada Plain	Ami'az Plain	Nahal Amazyahu
Max. dike H (m)	10	10	30	3
Max. dike width (m)	0.2	0.2	0.4	0.1
Branching	+	+	+	+
Dikelets	+	+	+	–
Intersection angle	–	Wide	70°–90°	Wide
Overlapping dike segments	–	+	+	–
Filling	Gray silt–clay	Gray silt–clay, pebbles	Gray silt–clay	Gray–green silt–clay
Dominant mineralogy (without clays)	cal, qtz, arag	cal, qtz, arag	cal, qtz, arag	cal, qtz, arag, dol, hal
Dominant clay mineralogy	kaol, IS	IS, kaol	IS, kaol	IS, kaol
Main AMS fabric	Injection	Injection	Injection	Injection
Source layer connection	+	–	+	–

Cal calcite, *qtz* quartz, *arag* aragonite, *dol* dolomite, *hal* halite, *kaol* kaolinite, *IS* illite–smectite

In the Bet ha'Arava study area, the clastic dikes are exposed in an area of $\sim$2.7 km^2 (Fig. 4a). They often exhibit vertical layers (foliation-like), reaching up to 10 m high and 0.2 m wide, and occasionally are associated with numerous dikelets. A connection of a green clay-rich layer of the Lisan Formation to the dike fill was observed. A few depositional dikes that crosscut the whole Lisan Formation up to the surface have a wedge-like shape, are about 0.1 m wide at their upper part, and become narrower at their lower part. Those dikes are filled by red brownish clay–silt material with a sporadic appearance of small pebbles. The strikes of the clastic dikes are scattered with clustering around NNE and NW–NNW directions (Fig. 5a). According to Gardosh (1987), several clastic dikes are emplaced in the Samra Formation (underlying the Lisan Formation) trending between NE and NNW directions.

In the Masada Plain study area, the clastic dikes are exposed in an area of $\sim$3.5 km^2 (Fig. 4b). The dikes are up to hundreds of meters long, up to 10 m high and 0.2 m wide. The dike infill consists of some pebbles derived from detritus, sometimes with a few vertical layers, Lisan layers, and discrete pieces of asphalt and oil films (Fig. 2e). The strikes of the dikes ($n = 130$) are scattered in a sector that ranges broadly from NE to W with possible clustering in a N to NNW direction (Fig. 5b).

The clastic dikes in the Ami'az Plain were mapped and studied by Marco et al. (2002) and Levi et al. (2006a, b, 2008, 2009, 2011) (Fig. 4c). The clastic dikes are exposed in an area of $\sim$3.5 km^2 and are mostly observed in the canyon walls of Nahal (Wadi) Perazim. The dikes are up to 1 km long, 30 m high, and 0.4 m wide (Levi et al. 2008). A connection of a green clay-rich layer of the Lisan Formation to the dike fill observed in several clastic dikes unequivocally indicates that the dikes were formed by injection of material from the clay-rich layer (Fig. 2a; Levi et al. 2006a). The strikes of the dikes ($n = \sim$250) are scattered in a broad sector ranging from ENE to W with slight clustering around a $\sim$NNW direction (Fig. 5c). Marco et al. (2002) showed that those clastic dikes are arranged mainly in a semi-radial and tangential geometry with more than 80 % of the intersections orthogonally.

The clastic dikes in the Nahal Amazyahu study area span an area of $\sim$1 km^2 (Fig. 4d). They are exposed only at the upper few meters of the Lisan section in canyon walls and at the flat tops of the gypsum layers. The dikes are up to hundreds of meters long, up to 3 m high and 0.1 m wide. The strikes of the dikes ($n = \sim$230) are scattered in a wide range of directions, with possible clustering around NE, W, and NW directions (Fig. 5d).

4.2 AMS results

Three types of AMS fabrics are observed. In Type A, all three AMS axes are well-grouped with horizontal to sub-horizontal k_1 axes parallel to the strike of the clastic dike (Fig. 6 sites AM-1; AM-4; AM-5; and Tn). In Type B, k_3 axes are well-grouped on the horizontal plane and k_1 and k_2 axes form a magnetic foliation (streaked pattern) roughly parallel to the strike of the clastic dike (Fig. 6 sites AM-2; AM-3; BA-1; MS-2; and BA-2). In sites BA-1, BA-2, and AM-3, k_2 axes are sub-vertical, whereas in site AM-2, k_2 axes are sub-horizontal. In Type C, k_1 axes are well-grouped on the horizontal plane and parallel to the strike of the clastic dike, and k_2 and k_3 axes form a magnetic foliation perpendicular to it (Fig. 6 sites MS-1 and BA-3).

Thermomagnetic curves show that the dominant magnetic carrier of the green clayey sediment of the dike and the source layer is the ferromagnetic mineral titanomagnetite (Levi et al. 2006a), which characterizes the Lisan Formation (Marco et al. 1998).

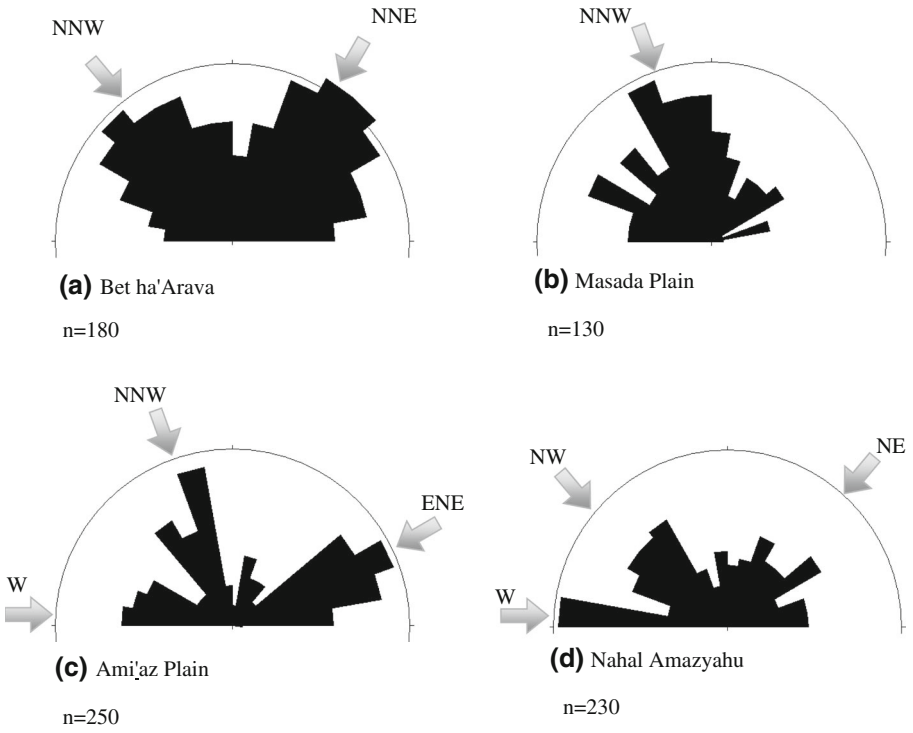

Fig. 5 Rose diagrams showing the distributions of clastic dike directions in the four study areas: **a** Bet ha'Arava ($n = 148$). Data were collected in the field by Gardosh (1987) and include only clastic dikes in the Lisan Formation. Data clustering is around NE and NW directions. **b** Masada Plain ($n = 130$, data collected in the field), showing a wide range of directions between NW and W (via north). A possible clustering is seen at NNW. **c** Ami'az Plain ($n = 250$, data collected in the field), showing a wide range of directions, which relate to semi-radial and tangential geometry of the clastic dikes (Marco et al. 2005). **d** Nahal Amazyahu ($n = 230$, data collected from air photographs), showing a wide range of directions with possible clustering at NE, W, and NW

4.3 Grain size and mineralogy

All samples from 10 clastic dikes and two layers show similar grain-size distribution and mineralogy (Table 2). The grain size ranges between 3 and 7 μm, indicating that the clastic material is "clay-rich sediment." The dominant minerals of the clastic material include mainly clays as well as calcite, quartz, dolomite, and feldspars. The clays are predominantly illite–smectite and kaolinite with minor amounts of illite. In Bet ha'Arava, we detected a relatively high concentration of kaolinite, and in the Ami'az Plain—dolomite and halite.

4.4 Simulation results

A quantitative simulation for evaluating liquefaction potential depends on a hypothetical PGV in the Ami'az Plain as noted in Sect. 3.4. The simulation results are presented in Fig. 7 and summarized as follows.

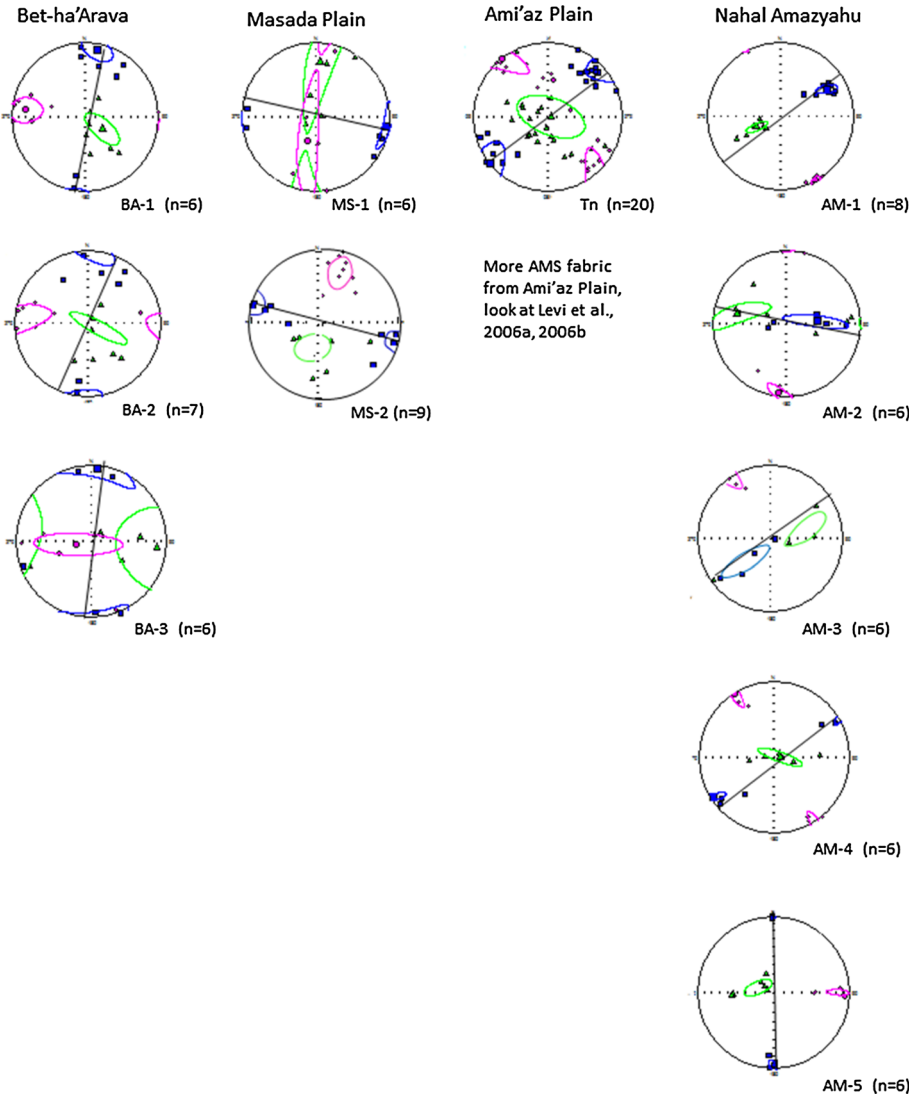

Fig. 6 AMS results of studied clastic dikes. Lower hemisphere, equal-area projections of AMS principal axes and the 95 % confidence ellipses, sector size 10°; *squares*, *triangles*, and *circles* represent the maximum (K_1), intermediate (K_2), and minimum (K_3) principal AMS axes, respectively. Dike strike is marked by a *solid line*. See details in text

1. The reference simulations with no an amplification factor (dashed lines) show moderate increase values of PGV at magnitudes of $M_w = 6$–7.5 and varied epicentral distances. Simulations with an amplification factor and epicentral distances of 60 and 90 km show a similar trend but with higher values of PGV.
2. For an epicentral distance ranges of 3, 10, 20 km for $M_w \geq 6$, and 40 km for $M_w \geq 6.5$, amplification conditions are required to produce liquefaction features.

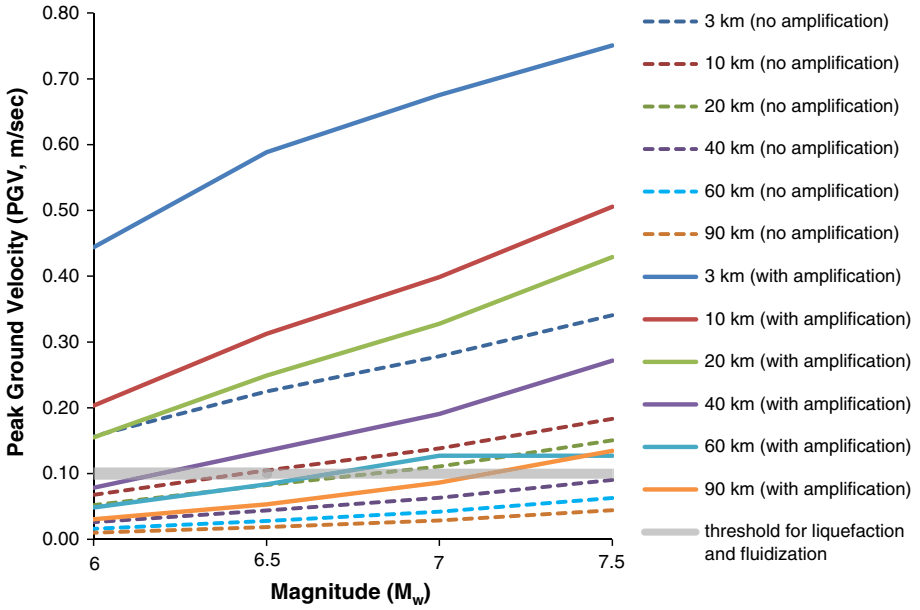

Fig. 7 Peak ground velocities (PGV) in Ami'az Plain for different earthquake magnitudes. PGV are based on the amplification factor 3 (Shani-Kadmiel et al. 2012) and the attenuation equation of Campbell and Bozorgnia, (2008) for strike-slip mechanism. Range of earthquake magnitudes (6–7.5 M_w) and epicenter distances (3, 10, 20, 40, 60, and 90 km) were applied. A *thick gray line* presents a threshold value above which PGV may enhance emplacement of clastic dikes by liquefaction (Cowan 1999; Kostadinov and Towhata 2002) and fluidization (Guo et al. 2006). The parameters used for the ground motion calculations are $M_w = 6$–7.5, orientation = 0°, dip angle = 90°, depth (ZTor) = 2 km, amplification factor = 3

Liquefaction can occur without amplification conditions only in cases of epicentral distances of 3 km for $M_w \geq 6$, 10 km for $M_w \geq 6.5$ and 20 km for $M_w \geq 7$.

3. For epicentral distances above 60 km with amplification conditions, the simulation results show that liquefaction features can be produced only for $M_w > 6.5$.
4. For epicentral distances with no amplification (40, 60, and 90 km), the simulation results show that liquefaction features are not likely to be produced.

5 Discussion

5.1 The origin of clastic dikes

The Lisan Formation covers vast areas ($\sim$300 km^2) along the western margin of the DSB (Fig. 1b). Yet, only in four, relatively small areas ($\sim$10 km^2) are clastic dikes observed (Fig. 1b). These dikes show similar characteristics in their geometry, infill material, AMS fabric, and spatial distribution and, hence, are likely to have a similar origin. There are several strong arguments for injection being the main mechanism in the four sites studied: (1) A physical connection exists between the clastic infill material and the clay-rich source layers, indicating upward flow (transport) of clastic material (e.g., Fig. 2). (2) Geometric features: The dikes are highly segmented mainly next to the uppermost gypsum layer,

forming a bunch of dikelets that attest to the dominance of a lateral direction of flow at the upper part of the Lisan Section. (3) A similar mineralogical assemblage and grain-size distribution exist in both the source layers and the clastic material in the dikes (Table 2). (4) The AMS analysis of the dike infill shows "flow fabrics" (Levi et al. 2006a), which are compatible with upward and lateral components of flow directions. The last two arguments are elaborated below.

A vertical sub-parallel layering of different materials within several clastic dikes indicates multiple injection events in the Ami'az Plain and the Masada Plain (Fig. 2f). There are no unequivocal criteria for determining whether a clastic dike was formed during a single event, or during multiple events.

Haliva-Cohen et al. (2012) studied the Lisan detritus and showed that it consists mainly of quartz and calcite grains with minor clays and feldspars, with typical grain sizes of 8–10 μm. The dike infill comprises similar detritus but with somewhat smaller grain sizes (3–7 μm), as opposed to sand dike infill with much coarser grain-size intrusions (Jolly and Lonergan 2002). The clay material of the dike infill consists mainly of illite–smectite and kaolinite. Compared to the results of Haliva-Cohen et al. (2012), the dike infill contains more kaolinite than the detritus in the Lisan Formation. Hence, the injected material of the source layers may have contained more kaolinite and smaller grain-size particles compared to the material within the source layer. This may indicate that relatively small grain-size particles of kaolinite are the preferred particles transported during the fluidization process (Arkin and Michaeli 1986). In the Ami'az Plain, the presence of dolomite and halite in the dike infill could be related to late authigenic mineral growth within the dike infill.

The AMS fabrics in Bet ha'Arava, the Masada Plain, and Nahal Amazyahu, and those studied previously by Levi et al. (2006a, b) in the Ami'az Plain, show a striking similarity (Fig. 6). All three types of AMS fabrics indicate that the clay-rich sediments were emplaced during flow conditions and not during deposition of clastics into open fissures. Based on the criteria provided by Levi et al. (2006a, b), the transport (flow) direction in Type A is parallel to k_2. This pattern serves as an indicator for turbulence flow under high velocity conditions and is commonly found in dikes that were emplaced between the source layer and the upper gypsum layers. Type B and Type C are interpreted as resulting from a turbulent flow that generates local eddies during the clastic transport. Tarling and Hrouda (1993) and Tauxe (1998) described streaked AMS patterns in sediment flow. They suggested that a streak pattern is caused by particles that are entrained under conditions of high-energy current flow. Consequently, due to rotation of particles during turbulent flow, k_1 axes in Type B are parallel to the strike of the clastic dike and k_2 axes indicate the flow direction (Levi et al. 2006b). In Type C, k_1 axes are parallel to the strike of the clastic dike and perpendicular to the flow direction and either k_2 or k_3 axes indicate the flow direction.

We conclude that the magnetic fabric analysis of the clastic dikes demonstrates that the AMS fabrics resulted from fast flow conditions, indicating that the transport of the dike infill was mainly upward. Occasionally, a lateral component of transportation was also involved, most commonly due to transport changes next to the stiff gypsum layers, which form a mechanical boundary for upward flow.

Levi et al. (2006b) showed that water content involved during fluidization could be relatively low and is not compatible with sand liquefaction, which seems to be associated with more water than that of fluidization. Therefore, the question whether local saturation of the Lisan sediments could be the main reason for fluidization and injection of clastic dikes in limited and small areas along the DSB is not an issue.

The shrinking and decline of the Lake Lisan level from its high stand (−180 m.s.l) to the low stand of the present Dead Sea (−420 m.s.l) started ~17,000 years B.P. (Haase-

Schramm et al. 2004) and continued until ~11,000 years B.P (Yechieli 1993). OSL ages (Porat et al. 2007) indicate that the clastic dikes in the Ami'az Plain were emplaced between 15,000 and 7,000 years B.P., overlapping the time interval of lake-level drop. During this lake-level drop, the top Lisan Formation was exposed and the groundwater level followed this lake-level drop. In each of the study areas, the exposure of the top Lisan Formation may have been at a somewhat different stage, depending on the elevation and tectonic deformation during the Holocene (Table 1). Bartov et al. (2002) determined shoreline elevations and reconstructed a lake-level curve. The groundwater-level drop was quite uniform along the shoreline over the entire area, and the exposure and desiccation of the Lisan soft rocks should not have varied too much over time and space. Hence, this could not explain conditions prevailing for fluidization at only four, relatively small and restricted sites.

5.2 The directions of the clastic dikes

The spatial distribution of the clastic dikes in each site may have been controlled by the local and/or regional stress field during the time of emplacement.

Unlike the hydro-fracturing mechanism, in Bet ha'Arava area, Gardosh (1987) suggested an integrated mechanism of clastic material deposition into giant desiccation fissures, whose strikes and opening direction were controlled by the regional stress field prevailing during the early Holocene. Indeed, based on analyses of various structures around the segment of the Dead Sea WBF system (Begin 1973; Raz 1983; Agnon 1983; Mor and Burg 2000; Sagy et al. 2003), geomorphic lineaments (Belitzky 1996; Shamir et al. 2005), linear clusters of collapse sinkholes (Wachs et al. 2000; Abelson et al. 2003), and earthquake focal mechanisms (Shamir 2006), it was suggested that post Pliocene, the stress field was characterized by two main directions of maximum compression, ~NNW–SSE and NE–SW. Likewise, the ~NNW–SSE direction was previously inferred as the regional maximum horizontal compression (σh_{max}) during and post Miocene (Eyal and Reches 1983; Eyal 1996; Eyal et al. 2001). Clustering of clastic dikes in those directions was observed also in Bet ha'Arava, the Masada Plain, and the Ami'az Plain. In this context, we discuss the strike direction patterns, in order to examine the possibility that the clustering of strikes of the clastic dikes in each study area was affected by the local stress field brought about by the underlying structures, or by a regional stress field.

In the Bet ha'Arava area, the directions of the clastic dikes are scattered widely with a bimodal distribution around NE and NNW directions (Fig. 5a). The clastic dikes are situated between the main strands of the DST: (1) ~3 km west of the Jericho Fault (~NNE striking); and (2) ~3.5 km east of the Dead Sea WBF (~NNW striking) and one of its secondary faults (~NNE striking, Fig. 3a). We suggest that the directions of the clastic dikes were weakly dictated by the local static stress field caused by those main faults during their emplacement into the stressed Lisan host rock at Bet ha'Arava.

The directions of clastic dikes in the Masada Plain are quite scattered, showing a wide range of directions from ~E to ~W. A possible clustering is seen around a NNW direction (Fig. 5b). This direction was also inferred from kinematic analysis of a set of faults next to the Dead Sea WBF (Sagy et al. 2003) and from recent lineaments of collapse sinkholes along the DSB (Abelson et al. 2003). Furthermore, the NNW trend is aligned sub-parallel to the local segment of the Dead Sea WBF (~1 km east); this direction is associated with the regional-scale (remote) stress field in the Dead Sea region. Taking into account that more than 50 % of the clastic dikes are randomly oriented (Fig. 5), it is suggested that during the dynamic injection of the clastic dikes in the Masada Plain, a static

stress field was weakly exerted by the local segment of the Dead Sea WBF, but had some minor effect on dike directions as indicated by the ~NNW clustering.

The directions of the clastic dikes in the Ami'az Plain are scattered, showing a wide range of directions from ~E to ~W. A possible clustering is seen around NNW, WNW, and ENE directions (Fig. 5c). This pattern may reflect unique deformation geometry in which the clastic dikes are arranged in semi-radial and tangential geometry (Marco et al. 2002). Marco et al. (2002) suggested that the radial traces converge eastward at the foot of the Sedom diapir, where a rising salt diapir is inferred (Zak 1967). This pattern could have been weakly controlled by a local static stress field exerted by the Ami'az sub-basin during the dynamic injection of clastic dikes.

Similar to the Ami'az Plain, the directions of the clastic dikes in Nahal Amazyahu are scattered, showing a wide range of directions from ~E to ~W. Clustering is observed at ~W and ~NW directions (~52 %; Fig. 5d). These two directions are at high angles to the main strand of the DST in this area. This strand, known as the Arava Fault, bisects the area, leaving most of the clastic dikes on its western side. The majority of these dikes form a semi-radial pattern converging at the fault trace. The distribution of clastic dikes in the Ami'az Plain and Nahal Amazyahu shows similarity in their radiating pattern. It is very possible that the wide scattering of the clastic-dike directions in these areas indicates that radial dynamic stress field is involved during the dike emplacement and earthquake events.

One possible explanation to the weak orientation clustering of clastic dikes might be related to an opening adjacent to a local geomorphological feature (e.g., parallel to a river bank or slope direction). In the studied sites, the clastic-dike orientations (Fig. 5) show no evidence of preferred clustering parallel to such local geomorphological features.

The dominant cause of scattering in orientations is most likely related to the dynamic stresses exerted by the high pressure evolving at the fluidized source layer and during the dike emplacement (Levi et al. 2008). The clustering around some directions could be dictated by local static stress fields, induced by adjacent structures (e.g., faults).

5.3 Spatial distribution of clastic dikes in the DSB clustering

The outcrops of the Lisan Formation cover an area of ~300 km^2 along the western margin of the DSB (Fig. 1b). Many of these outcrops are situated next to major strands of the DST (Fig. 1a), but in most of them, injection clastic dikes were not emplaced. The outcrops of clastic dikes at the western margin of the DSB cover only ~11 km^2, which is <4 % of the total outcrop area of the Lisan Formation. These areas show no greater proximity to the strands of the DST than other, dike-free Lisan outcrops. Hence, there could have been one or more significant elements that triggered emplacement of clastic dikes only in these four documented sites.

Liquefaction and fluidization features may vary from place to place in geometry, type, and dimensions. The variations may be due to different site conditions (e.g., grain size and density of deposits, position of the groundwater level) that might cause anomalous propagation and amplification of the seismic waves at the surface (Galli 2000). Because the studied clastic dikes are injection features that were emplaced in four isolated areas, amplification-driven fluidization seems a likely mechanism to explain the dike distribution, as discussed below.

Several conditions may cause amplification of the seismic waves during earthquakes in sedimentary basins such as the DSB. These conditions include the following (Shani-Kadmiel et al. 2012): (1) basin-wide amplification due to resonance and inelastic effects (Bard and Bouchon 1985; Semblat et al. 2002); (2) amplification above steep structures, i.e., faults due to an edge effect (Kawase 1996; Graves et al. 1998; Pitarka et al. 1998); and (3) amplification above sub-basins due to localized geometrical focusing (Graves et al. 1998; Semblat et al. 2002; Shani-Kadmiel et al. 2012). In sedimentary basins, where a lens of soft sediments overlies stiff rocks with higher seismic velocities, two-dimensional resonance patterns may prolong the duration of the ground shaking and induce high amplification. This was shown both in simulations (Bard and Bouchon 1985; Frankel and Stephenson 2000; Olsen 2000) and in field measurements (Field 1996; Joyner 2000; Frankel et al. 2002; Pratt et al. 2003). Shani-Kadmiel et al. (2012) used instrumental data with synthetic data based on computational modeling (Shani-Kadmiel et al. 2012, Fig. 2), in order to study the effects of earthquake ground motion in the sedimentary basins of the Ami'az Plain and the Masada Plain. Shani-Kadmiel et al. (2014) used analytical and numerical modeling in order to study the effects of geometrical focusing as a mechanism for significant amplification of ground motion in sedimentary basins. Their results indicate conclusively that the geometric features in the basin caused a complex pattern of ground motion amplification. Begin et al. (2005) studied the dimension of Breccia beds (seismites) within the Lisan Formation as an indication of the different local basin effects between the Ami'az Plain and the Masada Plain. They concluded that the differences in thickness of the Lisan seismites reflect specific basin response to strong earthquakes. Breccia beds in the Lisan Formation formed during the last 60,000 years were interpreted as seismites induced by $M > 5.5$ earthquakes (Marco and Agnon 1995; Marco et al. 1996; Marco and Agnon 2005). Marco et al. (1996) presented columnar sections of the Lisan Formation from the Masada and Ami'az Plains, exhibiting some 30 seismites that were formed by the same set of earthquakes. The seismites of the Ami'az Plain (Fig. 1b) are consistently thicker than those of the Masada Plain, even though 11 strong earthquakes from the recorded set occurred just north of the Masada Plain, which is much further north than the Ami'az Plain (Begin et al. 2005).

The geological structures and potential seismic reflectors (such as bedrock or fault plane) underneath each one of the four studied sites are diverse. Based on Shani-Kadmiel et al. (2012, 2014), the seismic reflectors as seismic sub-basins and steep faults generate an edge effect that may significantly amplify near surface ground velocity and trigger clastic-dike injection. In Bet ha'Arava and the Masada Plain, there is a relatively shallow salt layer (<0.5 and 1.1 km, respectively; Fig. 3a and Fig. 3b) above a steep normal fault, suggesting an edge effect. In the Ami'az Plain, the study area is located above a salt layer at a depth between 1.6 and 1.8 km with a southward plunging syncline, blocked from the northern side and bordered from the east and west by normal faults. This structure creates a wave-focusing sub-basin (Fig. 3c). In Nahal Amazyahu, the study area is located over the top Judea Group at a depth of 2.8 km and a steep normal fault (Fig. 3d) and, hence, also suggests an edge effect.

The simulations in this study indicate that the prerequisite for ground motion amplification for clastic-dike emplacement includes the following: (1) an earthquake magnitude between 6 and 7.5 M_w; (2) an epicentral distance of <50 km; and (3) amplification conditions. Without the amplification conditions, clastic dikes could be emplaced only in cases of epicentral distances of 3 km for $M_w \geq 6$, 10 km for $M_w \geq 6.5$, and 20 km for $M_w \geq 7$.

Hence, it is not likely that the deformation could be explained only by the vicinity to the epicenter location. Galli (2000, and references therein) demonstrated a similar conclusion

by empirical relationships to distance between liquefaction sites of historical earthquake epicenters. These relationships may be considered a tool for evaluating the minimum energy of an earthquake that induced liquefaction features. These arguments support the conclusion that basin amplification effects are one of the main triggering mechanisms for the fluidization process in the DSB.

Based on the explanations above, it is most likely that dike injection as well as other seismites in the Ami'az Plain and Masada Plain was emplaced by strong amplification (≥ 3) of ground motion during seismic events. Liquefaction and fluidization features are likely to be produced in moderate magnitude ($M_w \leq 6.5$) within epicentral radius <60 km, as well as in high magnitude ($M_w > 6.5$) within epicentral radius of more than 60 km.

Based on field observations, mineralogy and AMS analyses, and previous studies (Levi et al. 2006a, b; Porat et al. 2007), we conclude that the clastic dikes are injection structures that were emplaced dynamically due to fluidization of clay-rich source layers during earthquakes between 15,000 and 7,000 years B.P. The injection of the fluidized clay-rich material into the dikes occurred simultaneously with dynamic fracturing in small and distinct sites, enhanced by basin amplification effects in special local structural conditions.

The injection of clastic dikes may serve as evidence for seismic processes such as amplification effects that occur close to active faults and in local basins. Therefore, it should be taken into account when considering earthquake hazards in the newly exposed soft-sediment and planned development on the shores of the DSB. At this stage, further study and sensitive mapping are required.

6 Conclusions

1. The clastic dikes emplaced along the western margins of the DSB are distinct and exposed in relatively small areas. Their emplacement is related to amplification of seismic waves (factor = 3) in specific sites up to 60 km away from an epicenter in moderate earthquakes ($M_w \leq 6.5$), and even more than 60 km away from an epicenter in strong earthquakes ($M_w > 6.5$).
2. The sites are characterized by edge and basin effects generated by special local structures such as faults.
3. The orientations of the clastic dikes were weakly determined by the local stress field during dynamic fracturing of the Lisan host rock.
4. The present study indicates that fluidization and injection of clay-rich clastic materials during earthquakes have been conspicuous phenomena throughout the DSB.
5. We recommend that in places along the western margins of the DSB, where urban and infrastructure development is planned, site amplification surveys should be conducted.

7 Data and resources

The Earthquake Catalog of the Geophysical Institute of Israel can be found at www.gii.co.il (last accessed January 2014).

Acknowledgments We thank the Israel Science Foundation for funding through Grant 1736/11 to SM. We thank V. Schenk, the chief editor of Natural Hazards, and we are indebted to Graham Borradaile and an anonymous reviewer for providing constructive and very helpful reviews. Thanks to Amir Sandler, from the Geological Survey of Israel, for help and interpretation of mineralogy by X-ray diffraction. Thanks to Rivka Amit from the Geological Survey of Israel, for help and advice in preparation and operation of the Mastersizer for the grain-size analyses.

Appendix

Circular statistic was analyzed following Borradaile (2003) and includes characterization of multi-modality orientation distribution by sifting the data into separate homogeneous unimodal subgroups in quantile—quantile linearized plot. Another statistic parameters that were calculated are circular mean orientation, mean resultant length, mean orientation, and circular variance.

1. Circular mean orientation: calculation of unit vector over range of 180°

$$R = \sqrt{(\sum \cos\theta i^2) + (\sum \sin\theta i^2)}$$

2. Mean resultant length: express the strength of the alignment in a quantitative manner.

$$\bar{R} = R/n$$

3. Mean orientation:

$$\tan\bar{\theta} = \frac{\sin\bar{\theta}}{\cos\bar{\theta}}$$

The following algorithm transfers the trigonometrically determined angle into an azimuth:

$$\text{If } \sin\bar{\theta} > 0 \text{ and } \cos\bar{\theta} > 0 \text{ then } \bar{\theta} = \arctan\frac{\sin\bar{\theta}}{\cos\bar{\theta}}$$

$$\text{If } \cos\bar{\theta} < 0 \text{ then } \bar{\theta} = \arctan\frac{\sin\bar{\theta}}{\cos\bar{\theta}} + \pi$$

$$\text{If } \sin\bar{\theta} < 0 \text{ and } \cos\bar{\theta} > 0 \text{ then } \bar{\theta} = \arctan\frac{\sin\bar{\theta}}{\cos\bar{\theta}} + 2\pi$$

4. Circular variance:

$$V_c = 1 - \bar{R}, \quad 0 \le V_c \le 1$$

5. Circular standard deviation:

$$v = \sqrt{[-2\ln(1 - v_c)]}$$

6. Preferred orientations: provided by quantile—quantile linearized plot of circular orientation distributions that presents sensitive graphic test of the degree of uniformity. The plot presents more objective than inspecting circular diagrams directly (Fisher 1993). Perfectly uniform orientation distribution would be plotted along the dashed line, whereas the systematic departures indicate preferred orientation.

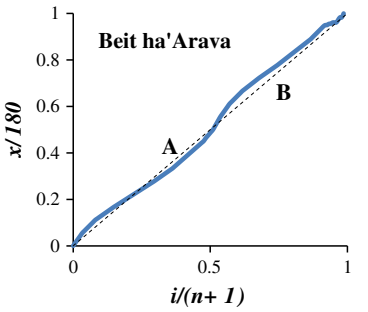

	Range	n	$\bar{R}$	V_c	$\bar{\theta}$	csd
A	40-90	47	0.91	0.09	62.2°	0.44
B	100-175	63	0.95	0.05	140.7°	0.32

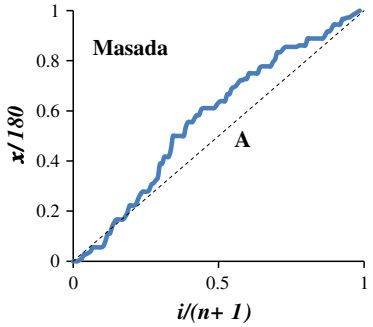

	range	n	$\bar{R}$	V_c	$\bar{\theta}$	csd
A	60-180	94	0.86	0.14	133.8°	0.54

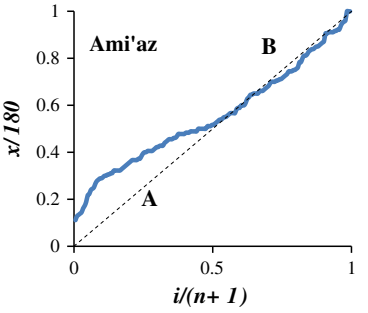

	range	n	$\bar{R}$	V_c	$\bar{\theta}$	csd
A	**20-110**	112	0.93	0.07	74.3°	0.38
B	**115-157**	49	0.96	0.04	134.4°	0.3

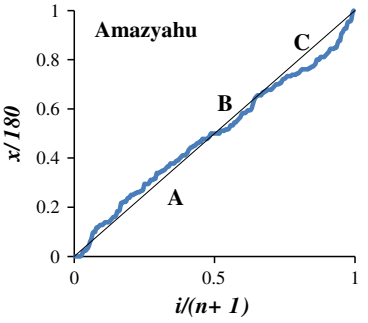

	range	n	$\bar{R}$	V_c	$\bar{\theta}$	csd
A	13-88	97	0.93	0.07	54.1°	0.38
B	90-118	42	0.98	0.02	100.7°	0.16
C	114-180	82	0.96	0.04	139.3°	0.28

The statistic circular orientations of the clustering include characterization of multi-modal. The statistic parameters that were calculated for Bet ha'Arava, Ami'az Plain, and

Nahal Amazyahu show a high mean orientation (>0.9); a low circular variance (<0.1); and a low standard deviation (<0.5). Orientations in Masada Plain are exceptional with a moderate standard deviation (0.54). The statistic circular orientations support the clustering results from the rose diagrams (Fig. 5).

References

Abelson M, Baer G, Shtivelman V, Wachs D, Raz E, Crouvi O, Kurzon I, Yechieli Y (2003) Collapse-sinkholes and radar interferometry reveal neotectonics concealed within the Dead Sea basin. Geophy Res Lett 30(10):1545. doi:10.1029/2003GL017103

Agnon A (1983) The development of sedimentary basins and morphotectonics in the southwestern margins of the Dead Sea. M.Sc. thesis (in Hebrew), Hebrew University, Jerusalem, Israel. 61 pp

Agnon A, Migowski C, Marco S (2006) Intraclast breccias in laminated sequence reviewed: recorders of paleo-earthquake. In: Enzel Y, Agnon A, Stein M (eds) New Frontiers in Dead Sea Paleoenvironmental Research. Geol Soc Am Bull, Special Publication 401:33–51. doi:10.1130/2006.2401(03)

Aldersons F, Ben-Avraham Z, Hofstetter A, Kissling E, Al-Yazjeen T (2003) Lower-crustal strength under the Dead Sea basin from local earthquake data and rheological modeling. Earth Planet Sci Lett 214(1–2):129–142. doi:10.1016/S0012-821X(03)00381-9

Alsop GI, Marco S (2011) Soft-sediment deformation within seismogenic slumps of the Dead Sea basin. J Struct Geol 33(4):433–457

Alsop GI, Marco S (2012) A large-scale radial pattern of seismogenic slumping towards the Dead Sea basin. J Geol Soc 169(1):99–110

Arkin Y, Michaeli L (1986) The significance of shear strength in the deformation of laminated sediments in the Dead Sea area. Isr J Earth Sci 35:61–72

Avni R, Bowman D, Shapira A, Nur A (2002) Erroneous interpretation of historical documents related to the epicenter of the 1927 Jericho earthquake in the Holy Land. J Seism 6(4):469–476

Bachrach R, Nur A, Agnon A (2001) Liquefaction and dynamic poroelasticity in soft sediments. J Geophys Res 106(B7):13515–13526

Bard PY, Bouchon M (1985) The two-dimensional resonance of sediment-filled valleys. Bull Seismol Soc Am 75:519–541

Bartov Y, Stein M, Enzel Y, Agnon A, Reches ZE (2002) Lake levels and sequence stratigraphy of Lake Lisan, the late Pleistocene precursor of the Dead Sea. Quat Res 57(1):9–21

Begin ZB (1973) The geological map of Israel (1:50,000). Jericho sheet, Geological Survey of Israel, Jerusalem

Begin ZB, Nathan Y, Ehrlich A (1980) Stratigraphy and facies distribution in the Lisan Formation - New evidence from the area south of the Dead Sea, Israel. Isr J Earth Sci 29:182–189

Begin ZB, Louie JN, Marco S, Ben-Avraham Z (2005) Prehistoric Seismic Basin Effects in the Dead Sea pull-apart. Geolologic Survey of Israel Report GSI/04/05, 38 pp

Belitzky S (1996) Tectonic geomorphology of the lower Jordan Valley: An active continental rift. Ph.D. thesis (in Hebrew, with extended English abstract), Hebrew University of Jerusalem

Belitzky S, Mimran Y (1996) Active salt diapirism at the Zahrat El-Qurein dome, lower Jordan Valley (Jordan). Isr J Earth Sci 45:11–18

Ben-Menahem A (1991) Four thousand years of seismicity along the Dead Sea rift. J Geophys Res 96:20195–20216

Borradaile GJ (1984) A note on sand dike orientations. J Struct Geol 6:587–588

Borradaile GJ (2003) Statistics of earth science data: their distribution in time, space and orientation. Springer, Berlin

Borradaile GJ, Henry B (1997) Tectonic applications of magnetic susceptibility and its anisotropy. Earth Sci Rev 42:49–93. doi:10.1016/S0012-8252(96)00044-X

Borradaile GJ, Jackson M (2004) Anisotropy of magnetic susceptibility (AMS): magnetic petrofabrics of deformed rocks. Geol Soc Lon Spec Publ 238(1):299–360

Campbell KW, Bozorgnia Y (2008) NGA ground motion model for the geometric mean horizontal component of PGA, PGV, PGD and 5% damped linear elastic response spectra for periods ranging from 0.01 to 10 s. Earthquake Spectra 24(1):139–171

Celebi M (1991) Topographical and geological amplification: case studies and engineering implification. Struct Saf 10:199–217

Cowan DS (1999) Do faults preserve a record of seismic slip? A field geologist's opinion. J Struct Geol 21:995–1001
Davis M (2007) The response of the lower Nahal Zin to base level changes and to the local bathymetry of Lake Lisan in the late Pleistocene and Holocene and landscape evolution of the northern Arava valley. M.Sc. Thesis (in Hebrew with English Abstr.), Hebrew University, Jerusalem, Israel, 58 pp
Eyal Y (1988) Sandstone dikes as evidence of localized transtention in a transpressive regime, Bir Zreir area, eastern Sinai. Tectonics 7:1279–1289
Eyal Y (1996) Stress field fluctuations along the Dead Sea Rift since the middle Miocene. Tectonics 15:157–170
Eyal Y, Reches Z (1983) Tectonic analysis of the Dead Sea rift region since the Late-Cretaceous based on mesostructures. Tectonics 2(2):39–66
Eyal Y, Gross MR, Engelder T, Becker A (2001) Joint development during fluctuation of the regional stress field in southern Israel. J Struct Geol 23:279–296
FEMA-NIBS (Federal Emergency Management Agency, National Institute of Building Sciences) (2012) Multihazard loss estimation methodology, earthquake model HAZUS-MH 2.1 technical manual, prepared for the Federal Emergency Management Agency, Washington, DC, United States, 676 pp
Fémények O, Diot H, Berza T, Gauffriau A, Demaiffe D (2004) Asymmetrical to symmetrical magnetic fabric of dikes: paleo-flow orientations and paleo-stresses recorded on feeder-bodies from the Motru Dike Swarm (Romania). J Struct Geol 26:1401–1418
Field EH (1996) Spectral amplification in a sediment-filled valley exhibiting clear basin- edge induced waves. Bull Seismol Soc Am 86:991–1005
Fisher NI (1993) Statistical analysis of circular data. Cambridge University Press, Cambridge 227 pp
Fleischer L, Gafsou R (1998) Top Judea Group – Digital structure map of Israel, Phase I (Arava Valley and Galilee). Geophysical Institute of Israel 873/90/97, 6 pp
Fleischer L, Bruner I, Gafsou R (2001) Top Judea Group – Digital structure map of Israel, Phase IV (Biqat Jericho). Geophysical Institute of Israe, 875/96/01, 8 pp
Frankel AD, Stephenson W (2000) Three-dimensional simulations of ground motions in the Seattle region for earthquakes in the Seattle fault zone. Bull Seismol Soc Am 90:1251–1267
Frankel AD, Carver DL, William RA (2002) Nonlinear and linear site response and basin effects in Seattle for the M 6.8 Nisqually, Washington, earthquake. Bull Seismol Soc Am 92:2090–2109
Freund R, Zak I, Garfunkel Z (1968) Age and rate of the sinistral movement along the Dead Sea Rift. Nature 220(5164):253–255. doi:10.1038/220253a0
Galli P (2000) New empirical relationships between magnitude and distance for liquefaction. Tectonophysics 324:169–187
Gardosh M (1987) Stratigraphy and tectonic activity of the Late Quaternary in the Dead Sea basin, M Sc. Thesis, Hebrew University, Jerusalem, Israel (in Hebrew, English abstr.), 73 pp
Garfunkel Z, Zak I, Freund R (1981) Active faulting in the Dead Sea rift. Tectonophysics 80(1–4):1–26. doi:10.1016/0040-1951(81)90139-6
Graves RW, Pitarka A, Somerville PG (1998) Ground-motion amplification in the Santa Monica area: effects of shallow basin-edge structure. Bull Seismol Soc Am 88(5):1224–1242
Guo Q, Liu H, Shen W, Yan X, Jia R (2006) Influence of sound wave characteristics on fluidization behaviors of ultrafine particles. Chem. Eng. J 119(1):1–9
Haase-Schramm A, Goldstein SL, Stein M (2004) U-Th dating of Lake Lisan aragonite (late Pleistocene Dead Sea) and implications for glacial East Mediterranean climate change. Geochim Cosmochim Ac 68:985–1005
Haliva-Cohen A, Mordechai S, Goldstein SL, Sandler A, Starinsky A (2012) Sources and transport routes of fine detritus material to the Late Quaternary Dead Sea basin. Quat Sci Rev 50:55–70
Hall JK (1993) The GSI digital terrain model (DTM) project completed. Israel Geological Survey, Current Research 8:47–60
Hamiel Y, Amit R, Begin ZB, Marco S, Katz O, Salamon A, Zilberman E, Porat N (2009) The Seismicity along the Dead Sea Fault during the Last 60,000 Years. Bull Seismol Soc Am 99(3):2020–2026. doi:10.1785/0120080218
Heifetz E, Agnon A, Marco S (2005) Soft sediment deformation by Kelvin Helmoltz Instability: a case from Dead Sea earthquakes. Earth Planet Sci Lett 236:497–504
Hofstetter A (2003) Seismic observations of the 22/11/1995 Gulf of Aqaba earthquake sequence. Tectonophysics 369(1–2):21–36. doi:10.1016/S0040-1951(03)00129-X
Hofstetter R, Klinger Y, Amrat AQ, Rivera L, Dorbath L (2007) Stress tensor and focal mechanisms along the Dead Sea fault and related structural elements based on seismological data. Tectonophysics 429(3–4):165–181. doi:10.1016/j.tecto.2006.03.010

Huang Q (1988) Geometry and tectonic significance of Albian sedimentary dykes in the Sisteron area, SE France. J Struct Geol 10:453–462
Israel National Oil Company (1992) Ami'az East-1 completion report. Geology. Tel Aviv, Various pagings, figs., maps, tabs, Section I
Israel National Oil Company (1999) Mezada and Tamar Licenses, petroleum potential and exploration strategy. Tel Aviv, Appen., fig., 38 pp
Jolly RJH, Lonergan L (2002) Mechanisms and controls on the formation of sand intrusions. J Geol Soc 159(5):605–617. doi:10.1144/0016-764902-025
Joyner WB (2000) Strong motion from surface waves in deep sedimentary basins. Bull Seismol Soc Am 90:69–83
Kawase H (1996) The Cause of the Damage Belt in Kobe: "The Basin-Edge Effect", Constructive Interference of the Direct S-Wave with the Basin-Induced Diffracted/Rayleigh Waves. Seismol Res Lett 67(5):25–34
Ken-Tor R, Agnon A, Enzel Y, Stein M, Marco S, Negendank JFW (2001) High resolution geological record of historic earthquakes in the Dead Sea basin. J Geophys Res 106:2221–2234
Klar A, Meirova T, Zaslavsky Y, Shapira A (2011) Spectral acceleration maps for 817 use in SI 413 amendment No. 5. GII Report No. 522/599/11 and NBRI 818, Report No. 2012938, 74 pp (in Hebrew)
Kostadinov MV, Towhata I (2002) Assessment of liquefaction-inducing peak ground velocity and frequency of horizontal ground shaking at onset of phenomenon. Soil Dyn Earthq Eng 22(4):309–322. doi:10.1016/S0267-7261(02)00018-0
Le Beon M, Klinger Y, Amrat AQ, Agnon A, Dorbath L, Baer G, Ruegg JC, Charade O, Mayyas O (2008) Slip rate and locking depth from GPS profiles across the southern Dead Sea Transform. J Geophys Res 113(B11). doi:10.1029/2007JB005280
Levi T, Weinberger R, Aïfa T, Eyal Y, Marco S (2006a) Earthquake-induced clastic dikes detected by anisotropy of magnetic susceptibility. Geology 34:69–72
Levi T, Weinberger R, Aïfa T, Eyal Y, Marco S (2006b) Injection mechanism of clay-rich sediments into dikes during earthquakes. Geochem Geophys Geosyst 7(2):1–20, Q12009, doi:10.1029/2006GC001410
Levi T, Weinberger R, Eyal Y, Lyakhovsky V, Heifetz E (2008) Velocities and driving pressures of clay-rich sediments injected into clastic dikes during earthquakes. Geophys J Int 175:1095–1107
Levi T, Weinberger R, Eyal Y (2009) Decay of dynamic fracturing based on three-dimensional measurements of clastic-dike geometry. J Struct Geol 31:831–841
Levi T, Weinberger R, Eyal Y (2011) A coupled fluid-fracture approach to propagation of clastic dikes during earthquakes. Tectonophysics 498(1):35–44
Loveless JP, Hoke GD, Allmendinger RW, González G, Isacks BL, Carrizo DA (2005) Pervasive cracking of the northern Chilean Coastal Cordillera: new evidence for forearc extension. Geology 33(12):973–976
Loveless JP, Allmendinger RW, Pritchard ME, Garroway JL, González G (2009) Surface cracks record long-term seismic segmentation of the Andean margin. Geology 37(1):23–26
Marco S, Agnon A (1995) Prehistoric earthquake deformations near Masada. Dead Sea graben. Geology 23(8):695–698
Marco S, Agnon A (2005) High-resolution stratigraphy reveals repeated earthquake faulting in the Masada Fault Zone. Dead Sea Transform. Tectonophysics 408(1–4):101–112
Marco S, Stein M, Agnon A, Ron H (1996) Long-term earthquake clustering: a 50,000-year paleoseismic record in the Dead Sea Graben. J Geophys Res 101(B3):6179–6191
Marco S, Ron H, McWilliams MO, Stein M (1998) High-resolution record of geomagnetic secular variation from late Pleistocene Lake Lisan sediments (paleo Dead Sea). Earth Planet Sci Lett 161:145–160. doi:10.1016/S0012-821X(98)00146-0
Marco S, Weinberger R, Agnon A (2002) Radial fractures formed by a salt stock in the Dead Sea Rift, Israel. Terra Nova 14:288–294
Marco S, Rockwell TK, Heimann A, Frieslander U, Agnon A (2005) Late Holocene activity of the Dead Sea Transform revealed in 3D palaeoseismic trenches on the Jordan Gorge segment. Earth Plan Sci Lett 234(1):189–205
McCalpin JP (1996) Paleoseismology. Academic Press, San Diego, International Geophysical Series 588 pp
Mor U, Burg A (2000) Geological map of Israel, Sheet 12-III, Mizpe Shalem, 1:50,000. The Geological Survey of Israel, Jerusalem
Moreira M, Geoffroy L, Pozzi JP (1999) Ecoulement magmatique dans les dykes du point chaud des Açores: étude préliminaire par anisotropie de susceptibilité magnétique (ASM) dans l'île de San Jorge. Comptes Rendus de l'Académie des Sciences-Series IIA-Earth Planet Sci 329(1):15–22

Neal TJ, Langer AM, Kerr PF (1968) Giant desiccation polygons of Great Basin playas. Geol Soc Am Bull 79(1):69–90
Neev D, Emery KO (1995) The destruction of Sodom, Gomorrah, and Jericho. Oxford University Press, Oxford
Obermeier SF (1998) Liquefaction evidence for strong earthquakes of Holocene and latest Pleistocene ages in the states of Indiana and Illonois, USA. Eng Geol 50:227–254
Olsen KB (2000) Site amplification in the Los Angeles basin from three-dimensional modeling of ground motion. Bull Seismol Soc Am 90:S77–S94
Olson SM, Green RA, Obermeier SF (2005) Geotechnical analysis of paleoseismic shaking using liquefaction features: a major updating. Eng Geol 76(3):235–261
Picard L (1943) Structure and evolution of Palestine. Hebrew University, Jerusalem, Geol Dep Bull 134 pp
Pitarka A, Irikura K, Iwata T, Sekiguchi H (1998) Three-dimensional simulation of the near-fault ground motion for the 1995 Hyogo-Ken Nanbu (Kobe), Japan, earthquake. Bull Seismol Soc Am 88(2):428–440
Pollard DD, Aydin A (1988) Progress in understanding jointing over the past century. Geol Soc Am Bull 100:1181–1204
Porat N, Levi T, Weinberger R (2007) Possible resetting of quartz OSL signals during earthquakes - Evidence from late Pleistocene injection dikes, Dead Sea basin, Israel. Quat Geochronol 2:272–277
Pratt TL, Brocher TM, Weaver CS, Creager KC, Snelson CM, Crossson RS, Miller KC, Trehu AM (2003) Amplification of seismic waves by the Seattle basin, Washington State. Bull Seismol Soc Am 93:533–545
Quennell A (1958) The structural and geomorphic evolution of the Dead Sea Rift. Quart J Geol Soc 114:1–24
Raz E (1983) The Geology of the Judean Desert, En-Gedi Area. Geological Survey of Israel, Jerusalem (in Hebrew, with English abstract) 110 pp
Reicherter K, Michetti A, PG Silva (eds) (2009) Palaeoseismology: historical and prehistorical records of earthquake ground effects for seismic hazard assessment. Geol Soc London, Special Publications, London
Sagy A, Reches Z, Agnon A (2003) Hierarchic three-dimensional structure and slip partitioning in the western Dead Sea pull-apart. Tectonics 22(1):1004–1021. doi:10.1029/2001TC001323
Semblat JF, Dangla P, Kham M, Duval AM (2002) Seismic site effects for shallow and deep alluvial basins: in-depth motion and focusing effect. Soil Dyn Earthq Eng 22(9–12):849–854
Serva L, Blumetti AM, Esposito E, Guerrieri L, Michetti AM, Okumura K, Porfido S, Reicherter K, Silva PG, Vittori E (2011) Earthquake Environmental Effects, intensity and seismic hazard assessment: the lesson of some recent large earthquakes. Earthquake Environmental Effects, intensity and seismic hazard assessment: the ESI intensity scale and the EEE Catalogue, Memorie Descrittive Carta Geologica d'Italia
Shamir G (2006) The active structure of the Dead Sea depression. In: Enzel Y, Agnon A, Stein M (eds) New Frontiers in Dead Sea Paleoenvironmental Research. Geol Soc Am Bull, Special Publications 401:33–51
Shamir G, Eyal Y, Bruner I (2005) Localized versus distributed shear in transform plate boundary zones: the case of the Dead Sea Transform in the Jericho Valley. Geochem Geophy Geosy 6:Q05004. doi:10.1029/2004GC000751
Shani-Kadmiel S, Tsesarsky M, Louie JN, Gvirtzman Z (2012) Simulation of seismic wave propagation through geometrically complex basins: the Dead Sea basin. Bull Seismol Soc Am 102(4):1729–1739. doi:10.1785/0120110254
Shani-Kadmiel S, Tsesarsky M, Louie JN, Gvirtzman Z (2014) Geometrical focusing as a mechanism for significant amplification of ground motion in sedimentary basins: analytical and numerical study. Bull Earthq Eng 12(2):607–625
Shapira A, Avni R, Nur A (1993) A new estimate for the epicenter of the Jericho earthquake of 11 July 1927. Isr J Earth Sci 42(2):93–96
Sneh A, Weinberger R (2014) Major Structures of Israel and Environs, scale 1:500,000. Geological Survey of Israel
Tarling DH, Hrouda F (1993) The Magnetic Anisotropy of Rocks. Chapman and Hall, London 217 pp
Tauxe L (1998) Paleomagnetic Principles and Practice. Springer, New York 299 pp
Vermilye JM, Scholz CH (1995) Relation between vein length and aperture. J Struct Geol 17:423–434
Wachs D, Yechieli Y, Shtivelman V, Itamar A, Bear G, Goldman M, Raz E, Rybakov M, Shatner U (2000) Formation of sinkholes along the shore of the Dead Sea. Geological Survey of Israel Report GSI/41/2000, 49 pp

Waldmann N, Starinsky A, Stein M (2007) Primary carbonates and Ca-chloride brines as monitors of a paleo-hydrological regime in the Dead Sea basin. Quat Sci Rev 26(17–18):2219–2228

Wdowinski S, Bock Y, Baer G, Prawirodirdjo L, Bechor N, Naaman S, Melzer Y (2004) GPS measurements of current crustal movements along the Dead Sea Fault. J Geophys Res 109:B05403. doi:10.1029/2003JB002640

Weinberger R, Begin ZB, Waldmann N, Gardosh M, Baer G, Frumkin A, Wdowinski S (2006) Quaternary rise of the Sedom Diapir, Dead Sea basin. In: Enzel Y, Agnon A, Stein M (eds) New Frontiers in Dead Sea Paleoenvironmental Research. Geol Soc Am Bull, Special Publication 401:33–51. doi:10.1130/2006.2401(03)

Yechieli Y (1993) The effects of water level changes in closed lakes (Dead Sea) on the surrounding groundwater and country rocks. Ph.D. Thesis, Weizman Institute of Science, Rehovot, Israel

Yılmaz MT, Pekcan O, Bakır BS (2004) Undrained cyclic shear and deformation behavior of silt–clay mixtures of Adapazarı, Turkey. Soil Dyn Earthq Eng 24:497–507

Zak I (1967) The geology of Mount Sedom, Ph.D. thesis, Hebrew University, Jerusalem (in Hebrew, English abstr.) 208 pp